AIAA JOURNAL
Vol. 44, No. 8, August 2006

Unsteady Wing-Body Aerodynamics for Aeroelastic Applications at Mach One

P. C. Chen* and D. D. Liu†
ZONA Technology, Inc., Scottsdale, Arizona 85258

DOI: 10.2514/1.15910

Renewed interest in the sonic-box method is prompted by the possibility of near-sonic flights. For aeroelastic applications, the sonic-box methods, however, would be hindered by their drawbacks/confinements. They are based on a velocity-potential formulation, thus the wake domain must be modeled for planforms with swept trailing edges or for multiple lifting surfaces; their nonplanar lifting surface application has not been demonstrated, nor has its flutter applicability; their extensions for bodies remain unexplored. To this end, an unsteady sonic methodology employing sonic acceleration potential for multiple lifting surfaces (wings) and sonic source velocity potential for bodies has been developed. The present unsteady sonic method should be recognized as the sonic counterpart of our previous development of the unsteady subsonic and supersonic wing-body methods. It will be shown that unsteady sonic methodology employing sonic acceleration potential is an expedient method for flutter/aeroelastic applications for wing-body configurations in the sonic/near-sonic Mach number range.

Introduction

WITH the advent of near-sonic transports including the once-conceived sonic cruiser, an expedient yet physical method for aeroelastic analysis at Mach one is paramount. Sonic flow, evaluated at Mach one does not strictly represent the flow physics at Mach one alone. The sonic-flow solution can be used for near-sonic flight applications in the close proximity of sonic Mach number. In fact, it has been shown by Landahl that the unsteady sonic equation is valid in this sonic flight range provided that his criterion [Landahl's criterion, inequality (4)] can be fulfilled. It turns out that Landahl's criterion for aeroelastic applications would largely qualify the modern supersonic/sonic aircraft design with moderate to low-aspect ratios, thin airfoil sections, and composite wings.

CFD methods in the last few decades are pursued as promising tools for unsteady transonic aerodynamics. CFD methods include the transonic small disturbance equation approaches, the full-potential approaches, to the current high-level Euler/Navier–Stokes approaches. However, computational inefficiency along with the grid-generation effort hinder these CFD methods as an expedient tool for industrial aeroelastic applications. On the other hand, as flow speed approaching sonic, the imbedded supercritical zone enclosed by sonic line and shock will enlarge and extend to the lateral far field. Thus in the sonic limit, proven supercritical transonic methods such as integral-method-based unsteady methods would cease to be applicable (e.g., [1,2]). For this reason, one seeks an expedient sonic method for industrial applications, which would represent the sonic counterpart of the proven unsteady transonic methods.

Unsteady Sonic Equation

The so-called time-linearized approach is to assume the oscillations amplitude as a small parameter that renders linearization of the unsteady flow equations. Hence, the time-linearized sonic equation in the frequency domain reads

$$\varphi_{yy} + \varphi_{zz} - 2ikM^2\varphi_x + k^2M^2\varphi = (\gamma+1)M^2\frac{\partial}{\partial x}[\phi_{0x}\varphi_x] \tag{1}$$

where k is the reduced frequency $k = \omega L/V$, L is the wing characteristic length, V is the free-stream speed, and ω is the oscillatory circular frequency. Note that the steady transonic flow velocity ϕ_{0x} enters here as a variant coefficient.

The parabolic sonic equation is one that generalizes the linear sonic equation with a replacement term to the coupling term on the RHS of Eq. (1) by $2\Gamma\phi_x$ [3], where 2Γ corresponds to the parabolic constant due to Oswatitsch [4]. Thus, Eq. (1) from here onward is approximated by the following

$$\varphi_{yy} + \varphi_{zz} + A\varphi_x + B\varphi = 0 \tag{2}$$

$$\text{where } A = -2(\Gamma M^2 + ikM^2),\quad B = k^2M^2,\quad \text{and}\quad \Gamma = \frac{\gamma+1}{2}M^2\phi_{0xx} \tag{3}$$

γ is the specific heat ratio; k is the reduced frequency based on chord length; M is the free-stream Mach number, and ϕ_{0xx} is the steady flow acceleration.

Based on the advanced wave dominant assumption (due to a sufficiently high reduced frequency), Landahl [5] derived the unsteady linear sonic equation by assuming $\Gamma = 0$. This assumption holds provided the reduced frequency is sufficiently high such that

$$k \gg \hat{\sigma}\tau\ \ell_n(\hat{\sigma}^{-1}\tau^{-1/3}) \tag{4}$$

where $\hat{\sigma}$ is the semi-span-to-chord ratio, and τ is the thickness ratio of the wing.

Inequality (4), or Landahl's criterion, is obtained based on an order of magnitude analysis which shows that the receding wave can be dissolved to an extent by a wing performing high-frequency oscillatory motions, hence the validity of the unsteady sonic equation.

For supersonic/sonic aircraft, it turns out that Landahl's criterion is usually satisfied for their flutter analysis because the low transonic drag requirement for high-speed flight requires a low-aspect ratio and small thickness ratio design. In later sections, we will show that indeed our flutter solutions can be well correlated with test data for cases that satisfy Landahl's criterion.

Analytical sonic-flow solution methods were based on the original linearized sonic equation of Lin et al. [6] derived from their order of

Received 2 February 2005; revision received 9 January 2006; accepted for publication 10 January 2006.

*Vice President; pc@zonatech.com. Member AIAA.
†Professor Emeritus, Arizona State University; danny.liu@asu.edu. Fellow AIAA.

magnitude analysis. Two-dimensional sonic solution of an oscillating airfoil based on this equation was given by Rott [7]. Landahl has subsequently developed the complete linear sonic-flow theory for wings and slender wing body [5]. Following Oswatitsch's parabolic methods [4], Liu et al. and Kimble et al. provide the linear sonic solution for bodies and wings with thickness effect, respectively [8,9]. The sonic kernel function method was provided by Runyan and Woolston [10] and Davies [11]. The sonic-box method was initiated by Andrew and Rodemich [12] and further extended by Olsen [13] and Ruo and Theisen [14]. Renewed interest in the sonic-box method has prompted the recent improvement of Soviero et al. [15].

Elementary Sonic Solution

Following Liu and Winther [3], the elementary solution of Eq. (2) at a field point (x_0, y_0, z_0) due to a point source with a unit strength at (x, y, z) can be expressed as

$$\begin{aligned}\Psi(\xi,\eta,\zeta) &= -\frac{1}{4\pi}e^{-[(B/A)\xi+(Ar^2/4\xi)]}/\xi \qquad \text{for } \xi \geq 0\\ &= 0 \qquad\qquad\qquad\qquad\qquad\quad \text{for } \xi < 0\end{aligned} \tag{5}$$

where $\xi = x_0 - x$, $r^2 = \eta^2 + \zeta^2$, $\eta = y_0 - y$, and $\zeta = z_0 - z$.

Equation (5) can be equivalently recast into the following, for $\xi \geq 0$,

$$\Psi(\xi,\eta,\zeta) = -\frac{1}{4\pi}e^{-(1/2)\bar{p}a\xi}e^{-(1/2)pM^2r^2/\xi}/\xi \tag{6}$$

where $p = \Gamma + ik$, $\bar{p} = -\Gamma + ik$, and $a = k^2/(\Gamma^2 + k^2)$.

It can be seen that Eq. (4) consists of two singularities at $\xi = 0$; one at $1/\xi$ and the other at $e^{-(1/2)PM^2r^2/\xi}$. In a later section, we will show that the $1/\xi$ type of singularity when appearing in the integral-solution format can be removed using integration by parts. The exponential singularity occurs also at $\xi = 0$ when Γ is set to zero. However, if Γ is first kept within P and in the limit, one can show that

$$\lim_{\Gamma\to 0^+} e^{-(1/2)pM^2r^2/\xi}|_{\xi=0} = 0$$

Hence, it is essential to carry through all Γ terms in our formulation for the sake of singularity treatment. This would justify our adoption of the unsteady parabolic sonic equation and solution, Eqs. (2) and (5). Note that Eq. (2) has been studied extensively and validated for low-aspect-ratio wing and bodies in the past [8,9,16]. Meanwhile, Eq. (5) can be considered a generalization of Landahl's unsteady sonic kernel (the elementary solution) in the sense that the parabolic constant Γ is treated as a mathematical artifice, if not as a physical/thickness parameter. It will be seen that Γ plays an important role throughout the subsequent formulation in the singularity removal for the sonic kernel.

Present Approach vs Sonic Box Methods

The sonic-box method, initiated by Rodemich et al. [12] and further extended by Olsen [13] and Ruo et al. [14] is confined to wing planforms modeled by rectangular boxes using the fundamental solution of the velocity potential [derivative of Eq. (6)]. Because of the rectangular integration domain imposed where ξ and η integrations are separable, analytical solution of the integral can be easily obtained. However, the leading and trailing edges of a swept wing cannot be precisely modeled by rectangular boxes, unless a large number of boxes is employed. Soviero and Cesar [15] introduced a quadrilateral box scheme that somewhat relieves this shortcoming of the sonic-box method. For industrial applications, sonic-box methods would be nevertheless hindered by the following drawbacks and confinements:

1) They are based on a velocity-potential formulation. Thus the wake domain must be modeled for planforms with swept trailing edges or for multiple lifting surfaces. If included, the wake domain would increase the box modeling effort even for a simple wing planform.

2) Their nonplanar lifting surface application has not been demonstrated, nor has its flutter applicability.

3) Their extensions for bodies remain unexplored.

To this end, an unsteady sonic methodology (ZSAP) employing sonic acceleration-potential for multiple lifting surfaces (wings) and sonic source velocity-potential for bodies has been developed. Note that the acceleration-potential formulation of the ZSAP has served as the basis for the doublet lattice method and for our previous subsonic/supersonic methods [17,18]. They are widely adopted by industrial practice for its wake-domain free input format. Hence, the present unsteady sonic method ZSAP should be recognized as the sonic counterpart of our previous development of the unsteady subsonic and supersonic wing-body methods [17,18]. It will be shown that ZSAP is an expedient method for aeroelastic applications for wing-body configurations in the sonic/near-sonic Mach number range.

Integral Equation for Wing-Body Configurations

For an arbitrary configuration, the solution of Eq. (1) at a point (x_0, y_0, z_0) can be obtained by solving the following integral equation:

$$\phi(x_0, y_0, z_0) = \phi_d + \phi_s$$

$$\phi_d = \iint_{S+W} \Delta\phi(x, y, z)(\boldsymbol{n}\cdot\nabla\Psi)\,\mathrm{d}s \tag{7}$$

is the unsteady doublet integral,

$$\phi_s = \iint_S \sigma(x, y, z)\Psi\,\mathrm{d}s \tag{8}$$

is the unsteady source integral, where $\Delta\phi$ is the velocity-potential distribution over the surface of the configuration S and the wake surface W, and σ is the unsteady source singularity distribution. Note that $\sigma = 0$ on the wake surface, and $\boldsymbol{n}$ is the out normal vector of the configuration surface.

For a lifting surface, the velocity potential $\Delta\phi$ can be recast into the acceleration potential by first defining an acceleration kernel integral:

$$K = \int_0^\xi e^{(1/2)P(a\lambda - M^2r^2/\lambda)}/\lambda^2\,\mathrm{d}\lambda \tag{9}$$

Next, performing integration by parts for ϕ_d by splitting the integrand of Eq. (7) into $\Delta\phi e^{-ika\xi}$ and $e^{(1/2)P(a\xi - M^2r^2/\xi)}/\xi^2$ which gives

$$\phi_d = \frac{PM^2\zeta}{8\pi}\left\{\int_\eta 2\Delta\phi e^{-ika\xi}K\Big|_0^{\xi L.E.}\mathrm{d}\eta + \iint_s \Delta\bar{c}_p e^{-ika\xi}K\,\mathrm{d}\xi\,\mathrm{d}\eta\right\} \tag{10}$$

where

$$\Delta\bar{c}_p = -2(\Delta\phi_x + ika\Delta\phi) \tag{11}$$

The first integral on the RHS of Eq. (10) vanishes because $\Delta\phi(\xi_{\text{L.E.}}) = 0$ at the lifting surface leading edge ($\xi_{\text{L.E.}}$) and $K(0) = 0$. The domain of the second integral only covers the configuration surface S. This is so because there is no flow acceleration on the wake-sheet; hence $\Gamma = 0$ and $a = 1$, thus leading to the reduced form of Eq. (11) on wake.

$$\Delta\bar{c}_p = -2(\Delta\phi_x + ik\Delta\phi)|_W = 0 \tag{12}$$

Equation (12) represents the zero pressure jump condition on the wake sheet, which completely eliminates the wake-sheet integral of Eq. (10). The unknown $\Delta\bar{c}_p$ on the configuration surface is in fact the acceleration potential that is solved together with the source singularity presently by the panel method.

Matrix Equation According to Panel Discretization

Following the same panel discretization scheme of ZONA6 and ZONA7, the surface of a wing-body configuration is broadly divided into two categories: the bodylike components and winglike components. The bodylike components, consisting of fuselage, external stores, tip tanks, etc., are discretized into quadrilateral boxes. These are called body boxes, whose leading and trailing edges are necessarily perpendicular to the x axis. Winglike components, consisting of lifting or flat surfaces such as wings, canards, fins, pylons, launches, etc., are discretized into trapezoidal boxes. These are called wing boxes, whose two side edges are necessarily parallel to the x axis. Figure 1 depicts such a panel discretization of a wing-body combination where the control point positions at the body boxes and wing boxes and their respective domains of influence are also shown. Note that the control points shown thereupon the wing and body boxes are best determined by numerical experiments at 99 and 50%, respectively, of the midchord of each box.

Assuming constant $\Delta\bar{c}_p$ and σ on each body box and wing box, respectively, Eq. (6) can be approximated as

$$\phi(x_0, y_0, z_0) = \sum_{i=1}^{\mathrm{NW}} \phi_{d_i} \Delta\bar{c}_{pi} + \sum_{i=1}^{\mathrm{NB}} \phi_{s_i} \sigma_i \tag{13}$$

where NW and NB denote the number of wing boxes and body boxes, respectively. ϕ_{d_i} is the potential influence coefficient (PIC) due to the ith wing box, and ϕ_{s_i} is the PIC due to the ith body box, that is

$$\phi_{d_i} = \frac{PM^2\zeta}{8\pi} \int_{\Delta\eta_i} \int_{\Delta\xi_i(\eta)} e^{-ika\xi} K \, \mathrm{d}\xi \, \mathrm{d}\eta \tag{14}$$

$$\phi_{S_i} = \int_{\Delta\xi_i} \int_{\Delta\eta_i(\xi)} \Psi \, \mathrm{d}\eta \, \mathrm{d}\xi \tag{15}$$

Applying the unsteady boundary condition at all wing and body boxes, the unknown $\Delta\bar{c}_p$ and σ can be obtained by solving the following matrix equation:

$$\begin{bmatrix} (\boldsymbol{n} \cdot \nabla\phi_{s_i})_{\mathrm{BB}}, & (\boldsymbol{n} \cdot \nabla\phi_{d_i})_{\mathrm{WB}} \\ (\boldsymbol{n} \cdot \nabla\phi_{s_i})_{\mathrm{BW}}, & (\boldsymbol{n} \cdot \nabla\phi_{d_i})_{\mathrm{WW}} \end{bmatrix} \begin{Bmatrix} \sigma \\ \Delta\bar{c}_p \end{Bmatrix} = \begin{Bmatrix} F_B \\ F_W \end{Bmatrix} \tag{16}$$

where

$(\cdot)_{\mathrm{BB}}$ is the influence at the body control points due to the body boxes,

$(\cdot)_{\mathrm{BW}}$ is the influence at the wing control points due to the body boxes,

$(\cdot)_{\mathrm{WB}}$ is the influence at the body control points due to the wing boxes,

$(\cdot)_{\mathrm{WW}}$ is the influence at the wing control points due to the wing boxes.

F_B and F_W are the downwash due to the structural oscillation at the body boxes and wing boxes, respectively. The detailed expressions of F_B and F_W can be found in Garcia-Fogeda et al. [19]. Once $\Delta\bar{c}_p$ and σ are obtained, the perturbation velocities $\nabla\phi$ can be computed by the superposition of $\nabla\phi_{s_i}$ and $\nabla\phi_{d_i}$ (called the velocity influence coefficient, VIC) with σ and $\Delta\bar{c}_p$, respectively, leading to the unsteady pressure solutions at all boxes.

Apparently, the crux of forming Eq. (16) lies on the integral solutions of ϕ_{s_i} and ϕ_{d_i}. As discussed earlier, the integrands of these integrals are singular at $\xi = 0$ which must be removed by analytical means.

Derivations of PIC and VIC for Wing Box

There are three integrals involved in ϕ_{d_i}: $\mathrm{d}\lambda$ in Eq. (9), $\mathrm{d}\xi$ and $\mathrm{d}\eta$ in Eq. (14), which have three different types of singularity, respectively. The integral of Eq. (9), by parts, can be split into two terms, that is,

$$K = (2/PM^2r^2)K_a - (a/M^2r^2)K_b \tag{17}$$

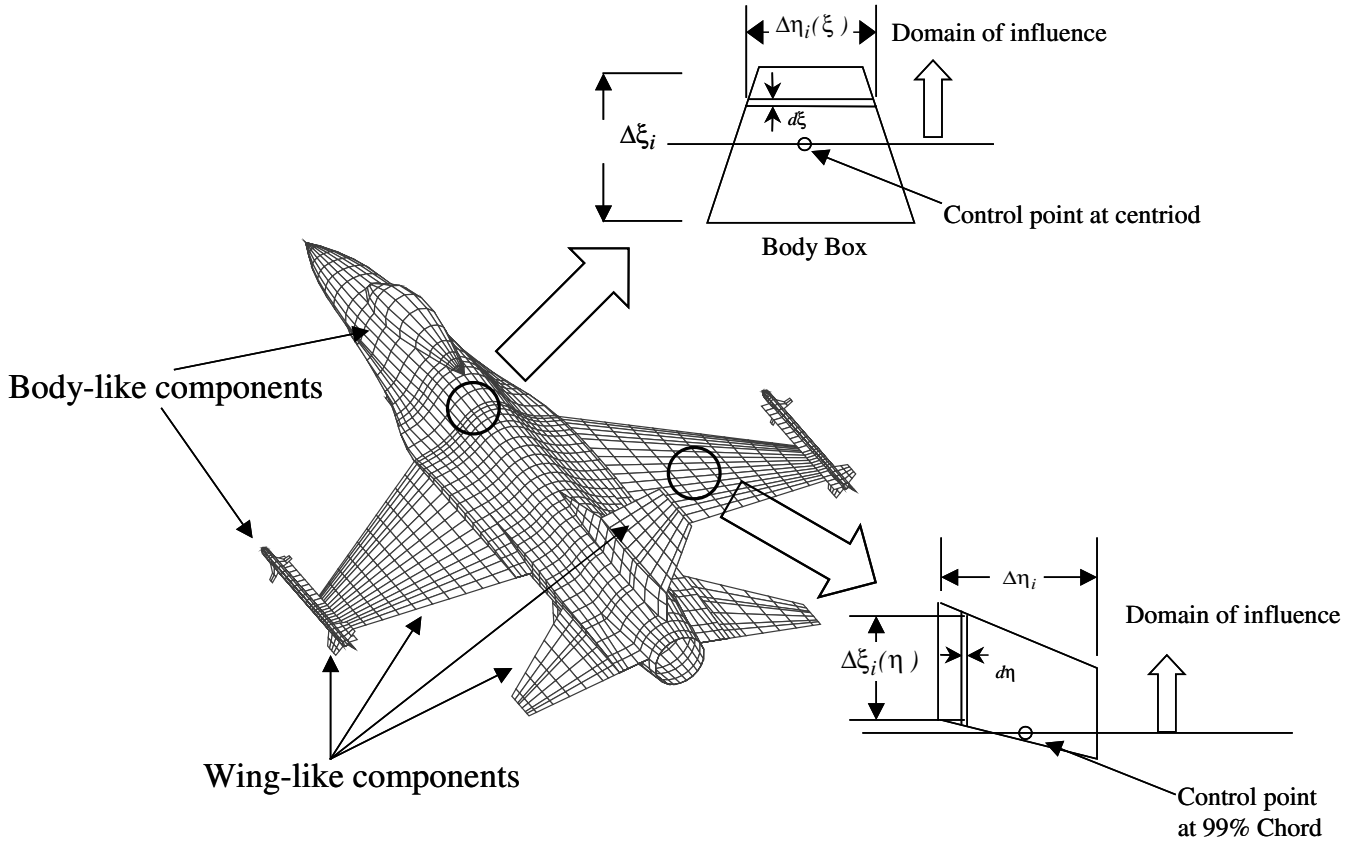

Fig. 1 Panel discretization of a wing-body configuration.

where

$$K_a = e^{(1/2)P(a\xi - M^2r^2/\xi)} \tag{18}$$

and

$$K_b = \int_0^{\xi} e^{(1/2)P(a\lambda - M^2r^2/\lambda)}\,\mathrm{d}\lambda \tag{19}$$

Note that Eq. (18) results from the upper limit of Eq. (9), whereas the lower limit vanishes based on Eq. (5). To obtain an analytical solution for K_b, the integral of Eq. (19) is split into two parts: a singular part defined as K_{b1} and a regular part defined as K_{b2}. Because an analytical solution exists for K_{b1}, that is

$$\begin{aligned} K_{b1} &= \int_0^{Mr/\sqrt{a}} e^{(1/2)P(a\lambda - M^2r^2/\lambda)}\,\mathrm{d}\lambda \\ &= \frac{1}{pa}\left\{1 + \rho - \frac{\pi}{2}[H_1(\rho) - Y_1(\rho)]\right\} \end{aligned} \tag{20}$$

where $\rho = P\sqrt{a}Mr$, $H_1(\rho)$ is the Struve function, and $Y_1(\rho)$ is the Weber function the singularity at $\lambda = 0$ is removed analytically. The regular part K_{b2} can be recast into a convenient expression ready to adopt Laschka's exponential approximation; that is

$$\begin{aligned} K_{b2} &= \int_{Mr/\sqrt{a}}^{\xi} e^{(1/2)P(a\lambda - M^2r^2/\lambda)}\,\mathrm{d}\lambda \\ &= \frac{1}{2a}\int_0^{-(a\xi - M^2r^2/\xi)}\left[\frac{\bar{u}}{\sqrt{\bar{u}^2+1}} - 1\right]e^{-(1/2)Pu}\,\mathrm{d}u \end{aligned} \tag{21}$$

where $\bar{u} = u/(2\sqrt{a}Mr)$

The Laschka's exponential approximation reads

$$1 - \bar{u}/\sqrt{\bar{u}^2+1} \approx \sum_{n=1}^{N} A_n e^{-C_n\bar{u}} \tag{22}$$

where the coefficients A_n, C_n, and N have been given by Laschka [20] and Desmarais [21].

Substituting Eq. (22) into Eq. (21) renders a series of simple exponential terms that can be immediately solved analytically. The $\mathrm{d}\xi$ integral of Eq. (14) contains a singular integral at $\xi = 0$ denoted as K_c, that is

$$K_c = \int_{\Delta\xi_i} e^{-(1/2)P(a\xi + M^2r^2/\xi)}\,\mathrm{d}\xi \tag{23}$$

The technique to remove the singularity of K_c is similar to that for K_b; that is, split into a singular part K_{c1} and a regular part K_{c2} where K_{c2} can be solved by numerical integration. An analytical solution of K_{c1} is also available that reads

$$K_{c1} = \int_0^{Mr/\sqrt{a}} e^{-(1/2)P(a\xi + M^2r^2/\xi)}\,\mathrm{d}\xi = -\frac{2}{P}\left\{e^{-\rho} + \rho K_1(\rho)\right\} \tag{24}$$

where $K_1(\rho)$ is the modified Bessel function of the second kind. The last integral of Eq. (14) involves a dipole-type singularity $(1/r^2)$ such as

$$\phi_{d_i} = \frac{PM^2\zeta}{8\pi}\int_{\Delta\eta} F(\eta)/r^2\,\mathrm{d}\eta \tag{25}$$

This dipole singularity also exists in both subsonic and supersonic integral equations [17,18,24] where a special numerical technique is available for removing such a singularity. This special numerical technique first approximates $F(\eta)$ by polynomials in terms of η then solves the resulting rational function analytically. Once the solution of ϕ_{d_i} is available, VIC of wing box can be obtained by taking the gradient of ϕ_{d_i}. For instance, the normal velocity W_{d_i} can be expressed as

$$W_{d_i} = \frac{\partial}{\partial Z_0}\phi_{d_i} = W_P + W_N \tag{26}$$

where $W_P = \phi_{d_i}/\zeta$ is the so-called planar normal velocity influence coefficient, and

$$W_N = \frac{-P^2M^4\zeta^2}{8\pi}\int_{\Delta\eta_i}\int_{\Delta\xi_i(\eta)} e^{-ika\xi}K_N\,\mathrm{d}\xi\,\mathrm{d}\eta \tag{27}$$

is the so-called nonplanar normal velocity influence coefficient.

K_N is the nonplanar part of the acceleration kernel integral K. It is very similar to K except it contains a $1/\lambda^3$ singularity but that can be also removed analytically using integration by parts.

Derivation of PIC and VIC for Body Box

Because an analytical solution exists for the inner integral of Eq. (15), ϕ_{s_i} can be immediately reduced to a single integral, that is

$$\phi_{s_i} = \left[-1\Big/\left(8\sqrt{\pi}\right)\right]\left(\sqrt{2}\Big/\sqrt{PM^2}\right)\int_{\Delta\xi} e^{(-1/2)\bar{P}a\xi}e^{(-1/2)PM^2\zeta^2/\xi}\,\mathrm{erf}\left[\sqrt{(\tfrac{1}{2}PM^2)/\xi}\eta\right]\Big/\sqrt{\xi}\Big|_{\eta_L(\xi)}^{\eta_U(\xi)}\,\mathrm{d}\xi \tag{28}$$

where erf is the error function and $\eta_L(\xi)$ and $\eta_U(\xi)$ denote η at the two side edges of the body box. Equation (28) contains a $1/\sqrt{\xi}$ singularity at $\xi = 0$, therefore, it cannot be solved by a straightforward numerical integration. It is known that the error function can be approximated by rational approximation such as

$$\mathrm{erf}\left[\sqrt{(\tfrac{1}{2}PM^2)/\xi}\eta\right] \approx 1 - \sum_{n=1}^{5} a_n(\xi^{n/2})\Big/\left[\sqrt{\xi} + q\sqrt{\tfrac{1}{2}PM^2}\eta\right]^n e^{(-1/2)PM^2\eta^2/\xi} + \varepsilon, \qquad |\varepsilon| < 1.5\times 10^{-7} \tag{29}$$

where a_n and q are constants whose values can be found in [23]. Substituting Eq. (29) into Eq. (28) yields two terms. The first term is independent of η and vanishes because of the cancellation between $\eta_L(\xi)$ and $\eta_U(\xi)$. In the second term the numerator $\xi^{n/2}$ arose from the rational approximation removes the singularity of order $1/\sqrt{\xi}$, rendering a regular function that is solvable by numerical integration.

The velocity influence coefficients ($\nabla\phi_{si} = U_i\boldsymbol{i} + V_i\boldsymbol{j} + W_i\boldsymbol{k}$) of the body box are shown as follows:

$$W_i = \partial\phi_{si}/\partial z_0 = \tfrac{1}{4}\sqrt{PM^2/2\pi}\int_{\Delta\xi}\zeta e^{(-1/2)\bar{p}a\xi}e^{(-1/2)PM^2\zeta^2/\xi}\mathrm{erf}\left[\sqrt{(\tfrac{1}{2}PM^2)/\xi}\eta\right]\Big/\xi^{3/2}\Big|_{\eta_L(\xi)}^{\eta_U(\xi)}\,\mathrm{d}\xi \tag{30}$$

$$V_i = \partial\phi_{si}/\partial y_0 = \frac{-1}{4\pi}\int_{\Delta\xi} e^{(-1/2)\bar{p}a\xi}e^{(-1/2)PM^2r^2/\xi}/\xi\Big|_{\eta_L(\xi)}^{\eta_U(\xi)}\,\mathrm{d}\xi \tag{31}$$

$$U_i = \partial\phi_{si}/\partial x_0 = \partial\phi_{si}/\partial\xi - s_i V_i - b_i W_i \tag{32}$$

where $\partial\phi_{si}/\partial\xi$ represents the integrand of Eq. (28). s_i denotes the slope of a side edge and b_i the inclination angle of the ith body box. In Eqs. (30) and (31), W_i contains a $1/\xi^{3/2}$ singularity and V_i contains a $1/\xi$ singularity at $\xi = 0$ but they can be removed analytically. For example, the integrand of Eq. (30) can be split into

$$(\zeta/\xi^{3/2})e^{(-1/2)PM^2\zeta^2/\xi} \quad \text{and} \quad e^{(-1/2)\bar{P}a\xi}\,\mathrm{erf}\left[\sqrt{(\tfrac{1}{2}PM^2)/\xi}\eta\right]$$

Because

$$\zeta\int_{\Delta\xi}[e^{(-1/2)PM^2\zeta^2/\xi}]/\xi^{3/2}\,\mathrm{d}\xi = \sqrt{(2\pi)/PM^2}\,\mathrm{erf}\left[\sqrt{(\tfrac{1}{2}PM^2)/\xi}\zeta\right] \tag{33}$$

and the rational approximation of the error function can remove a singularity of order $1/\sqrt{\xi}$, the $1/\xi^{3/2}$ singularity can be eliminated by a sequence of integration by parts. Thus, the resulting integrals can be solved by numerical integration.

It is well known that a source sheet produces a flow field where the normal velocity is discontinuous across the sheet while the tangential velocity as well as the potential are continuous. To verify that this is also the case for the sonic flow, let us consider a body box with zero inclination angle so that W_i is the normal velocity of the box. When a point (x_0, y_0, z_0) approaches the body box from the upper and lower sides, that is $\xi \to 0$ and $\zeta \to 0^{\pm}$, the error function in Eq. (33) resulting from integration by parts produces a discontinuity such as

$$\lim_{\zeta\to 0^{\pm}}\lim_{\xi\to 0}\mathrm{erf}\left[\sqrt{(\tfrac{1}{2}PM^2)/\xi}\zeta\right] = +1 \quad \text{for } \zeta = 0^{+}$$
$$= -1 \quad \text{for } \zeta = 0^{-} \tag{34}$$

Since such an error function only appears in the solution of the W_i integral indicating that W_i is discontinuous whereas U_i, V_i, and ϕ_{s_i}, are continuous across the source sheet, Eq. (34) verifies the correct behavior of the source integral solutions for the body boxes.

Validations for Winglike Components

Five lifting surface cases are selected for validation of the present sonic-freeze acceleration-potential (ZSAP) method. The planforms include delta wings, a rectangular wing, and a nonplanar canard-wing configurations where the lift and moment stability derivatives and generalized aerodynamic forces are compared with other analytical and numerical results.

Damping-In-Pitch of Delta Wings

Two delta wings of aspect ratios $A = 1.5$ and $A = 3.0$ are selected for damping derivative computations. A pitching axis is located at 60% root chord for both cases. Figure 2 shows the damping-in-pitch moment derivatives versus reduced frequencies computed by ZSAP, Landahl's third order theory [5] and Ruo and Theisen's sonic-box method [14].

It is seen that the present solution is in better agreement with Landahl's solution than with the Ruo and Theisen's solution for the aspect ratio 1.5 case. For the aspect ratio 3.0 case, the present method correlates better with the Ruo and Theisen's solution. This is expected because the present method is generally valid for all aspect ratios. Landahl's third order theory serves as an asymptotic limit towards the low-aspect-ratio end; it tends to be inaccurate as the aspect ratio increases. On the other hand, the sonic-box method suffers from the solution inaccuracy on low-aspect-ratio wings because the high swept leading edge of the low-aspect-ratio delta wing can not be accurately modeled by a finite number of rectangular boxes. However, because this problem is partially relieved as the leading edge swept angle decreases, the sonic-box method tends to provide better solution accuracy on high aspect ratio wings.

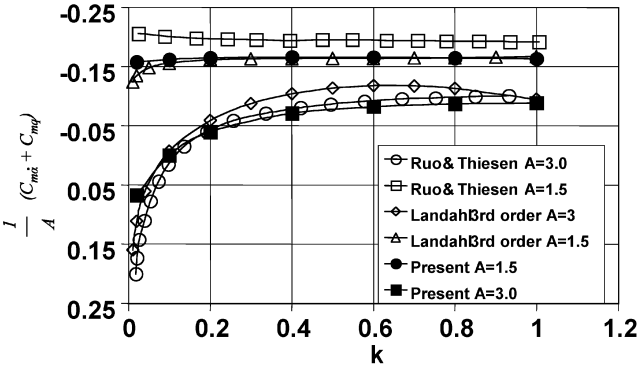

Fig. 2 Damping-in-pitch derivatives vs k for delta wings of aspect ratios $A = 1.5$ and $A = 3.0$.

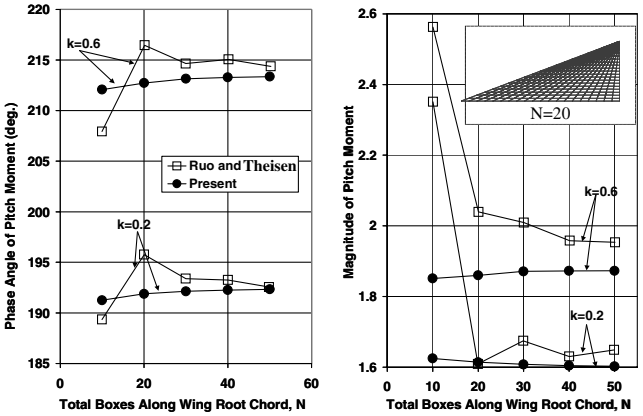

Fig. 3 Pitching moments of delta wing ($A = 1.5$) versus chordwise boxes.

Solution Convergence for Pitch Moment of Delta Wing

The objective of the solution convergence study is to demonstrate that the present method is insensitive to the number of boxes. The pitching moments of the delta wing of aspect ratio $A = 1.5$ oscillating about its apex at two reduced frequencies; $k = 0.2$ and 0.6, are computed by the present method and the Ruo and Theisen's sonic-box method. Figure 3 shows the phase angle and magnitude of the pitching moments at various chordwise boxes "N" while the spanwise boxes are kept at 20. It can be seen that the solution of the sonic-box method is highly oscillatory at low N and still not converged at $N = 50$. This slow solution convergence of the sonic-box method is again caused by its inaccurate modeling problem for low-aspect-ratio wings. By contrast, the present solution appears to be insensitive to the box number chosen, showing that ZSAP is a more robust method.

Lift Because of Plunging/Pitching Motions at Various Reduced Frequencies

Figures 4 and 5 present the lift coefficients due to a plunging delta wing ($A = 1.5$) and a pitching rectangular wing ($A = 2.0$) about its leading edge, respectively. The ZSAP solutions in terms of the lift magnitude and phase angle of C_{L_α} are compared with Landahl's third order solutions and those of sonic-box methods due to Rodemich and Andrew [12] and Soviero et al. [15,22].

Here, almost all solution for the in-phase lift are uniformly valid throughout the frequency domain. For the delta wing case, in Fig. 4 all solutions approach the same limiting value at $k = 0$, except the magnitude of lift computed by Rodemich and Andrew, showing the validity of Landahl's third order solution as a benchmark. Again in Fig. 5, all solutions approach the same limiting value at $k = 0$ for a pitching rectangular wing.

For values of k beyond 0.2, larger discrepancies are found among different solutions for the rectangular wing (Fig. 5) case than the delta

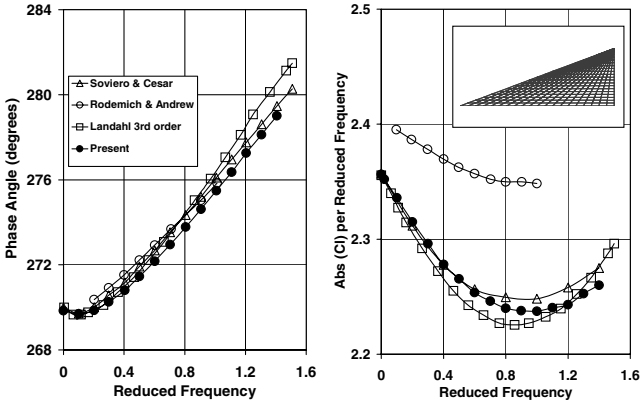

Fig. 4 Lift on a delta wing ($A = 1.5$) versus k.

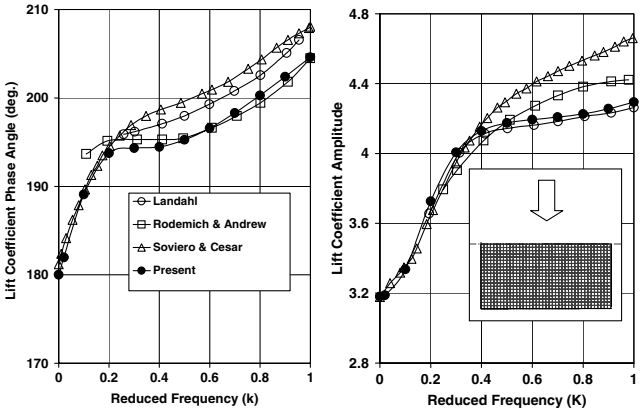

Fig. 5 Lift on a rectangular wing ($A = 2.0$) versus k.

wing case (Fig. 4). The departures of the sonic-box solutions from that of ZSAP are perhaps caused by the difference in the formulation as to how the upstream sonic wave is being collected by each control point.

Nonplanar Aerodynamics of Saab Canard-Wing Configuration

The objective of this case is twofold: 1) to demonstrate the present ZSAP method's nonplanar capability, 2) to show the solution robustness of the present method at $M = 1.0$ whereas other subsonic and supersonic methods require a large number of boxes for solution convergence at Mach number near one.

Here, the Saab canard-wing configuration (Fig. 6) is an idealization of the Saab 37 Viggen canard airplane whose dimensions can be found in Stark [26]. The case considered is a pitching canard about its midchord while the main wing below is kept stationary. In this case, the lift on the main wing is mainly induced by the oscillatory wake from the canard; rendering an ideal case for validating nonplanar aerodynamics.

The lift on the main wing due to the canard pitch oscillation can be obtained from the generalized aerodynamic force matrix and is denoted here as Q_{12}. Q_{12} at various reduced frequencies are computed by using the present method at $M = 1$, the subsonic unsteady aerodynamic method ZONA6 at $M = 0.99$, and the supersonic unsteady aerodynamic method ZONA7 at $M = 1.01$. It is well known that the subsonic and supersonic integral equations involve a parameter $k/|1 - M|^{1/2}$, called the compressible reduced frequency, which becomes very large when M approaches one. In this condition, the unsteady pressure distribution becomes highly oscillatory due to the large compressible reduced frequency, implying that a large number of boxes is required for solution convergence for ZONA6 and ZONA7. However, this is not the case for the present method because of the absence of the compressible reduced frequency in the sonic equation.

Shown in Fig. 6a are the ZSAP solution versus the ZONA6 and ZONA7 solutions at various reduced frequencies using a 10×10 box modeling for the canard and a 20×20 box modeling for the main wing. It is seen that both ZONA6 and ZONA7 solutions diverge when $k > 1$ whereas the ZSAP solutions appear to remain smooth. This suggests that this box modeling is too coarse for a converged ZONA6/ZONA7 solution due to the compressible reduced frequency effects. This can be verified by results shown in Fig. 6b where the box numbers are increased to 50×10 for the canard and 90×20 for the wing. In this case, the subsonic/supersonic solutions converge to the ZSAP solution as expected. Meanwhile, comparing the solutions obtained on the coarse box model to these on the refined box model, it can be seen that these two sets of ZSAP solutions are practically the same, indicating that the ZSAP solution has already converged on the coarse box model.

Validation for Bodylike Components

A 12.5° cone at $M = 1$ is selected as the test case for validating the body box modeling. Figure 7 presents the damping-in-pitch moment derivative of the cone with various pitch axis locations. The ZSAP results are compared with those of the Liu's quasislender body theory [27], Landahl's theory [28], and the slender body theory where good agreement between the ZSAP results and Liu's results is seen. Note that Liu's quasislender body includes the fourth order body thickness effects whereas Landahl's theory is a second order theory and the slender body theory is only first order. Therefore, the good agreement between the ZSAP results and Liu's results is expected because the ZSAP body box formation accounts for any arbitrariness of the body shape; that is, body thickness effect is fully included.

The accuracy of the ZSAP body box formulation is further validated with the damping-in-pitch force derivative of the 12.5° cone. Shown in Fig. 8 is the comparison of the force derivative at various reduced frequencies between the ZSAP results and Liu's results. Again, good agreement is obtained.

Validation for Flutter Solutions

Almost all sonic-flow research works stopped at the unsteady aerodynamic level. Apparently, no flutter solution has been given as a continued verification of the analytical or numerical methods. However, the major thrust on the sonic method should lie in the expedient aeroelastic application. To this end, the AGARD 445.6 wing wind-tunnel measurements and the flight test data of a F-16 aircraft with external stores are selected to validate the flutter solutions of the present method.

AGARD 445.6 Wing

Served as a standard transonic flutter solution benchmark case, the AGARD 445.6 wing [29] and its wind-tunnel measured tunnel boundaries have been adopted for validating many CFD methods. Here, we merely attempt to validate the ZSAP flutter solutions at Mach one.

Two different structures of the AGARD 445.6 wing are selected: the weakened wing (tested in air) and the solid wing (testing in Freon 12). Figure 9 presents the ZSAP flutter solutions at $M = 1$ expressed in terms of the flutter speed index $U/(b_s\omega_\alpha\sqrt{\mu})$ and the flutter frequency ratio ω/ω_α along with the wind-tunnel measured flutter boundaries. Excellent agreement with the test data for both weakened and solid wings at Mach one is obtained. This excellent agreement is by no means a coincidence because the low thickness ratio of the AGARD 445.6 wing warrants the validity of the linearized sonic equation. The semi-span-to-chord ratio $\hat{\sigma}$ of the AGARD 445.6 wing is 1.36 whereas the thickness ratio $\tau = 0.04$. This gives the RHS of Eq. (4) a value of $\hat{\sigma}\tau\ \ell_n\ \hat{\sigma}^{-1}\tau^{-1/3} = 0.0416$. The reduced frequencies of the ZSAP flutter solution are 0.07 for the weakened wing and 0.17 of the solid wing; both satisfy the inequality equation presented in Eq. (4) which fully justify the present flutter solutions.

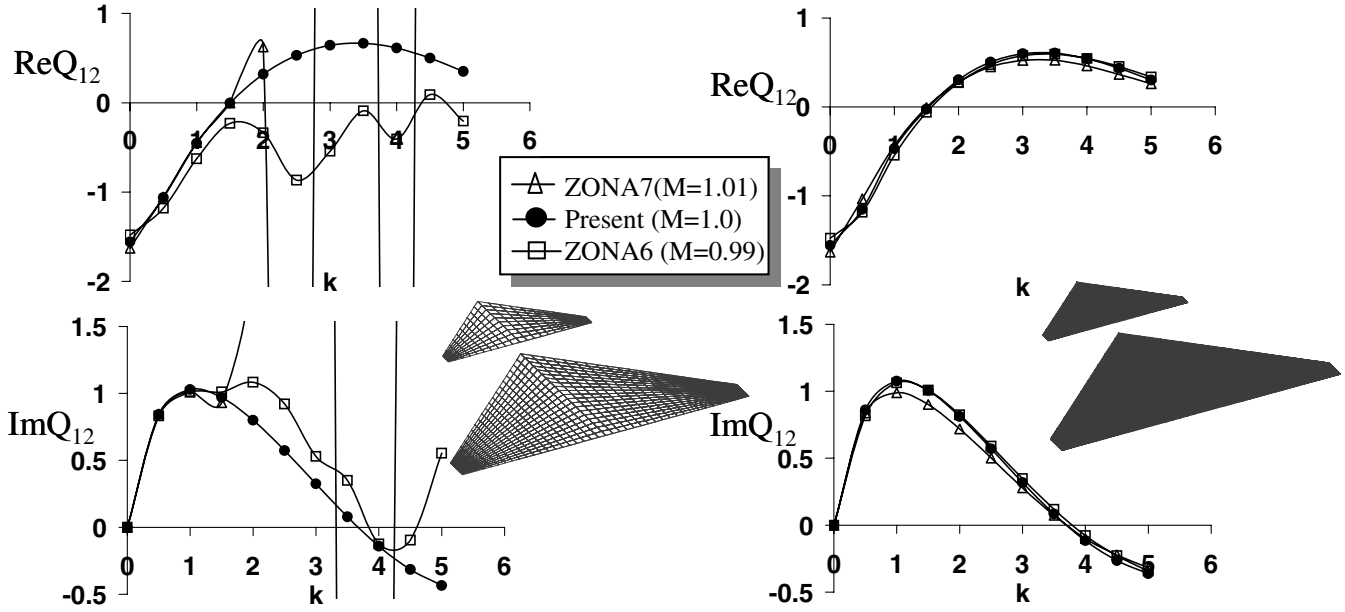

(a) Box Number 10 x 10 for Canard & 20 x 20 for Wing (b) Box Number 50 x 10 for Canard & 90 x 20 for Wing

Fig. 6 Lift on main wing due to canard pitch oscillation on a Saab canard-wing configuration.

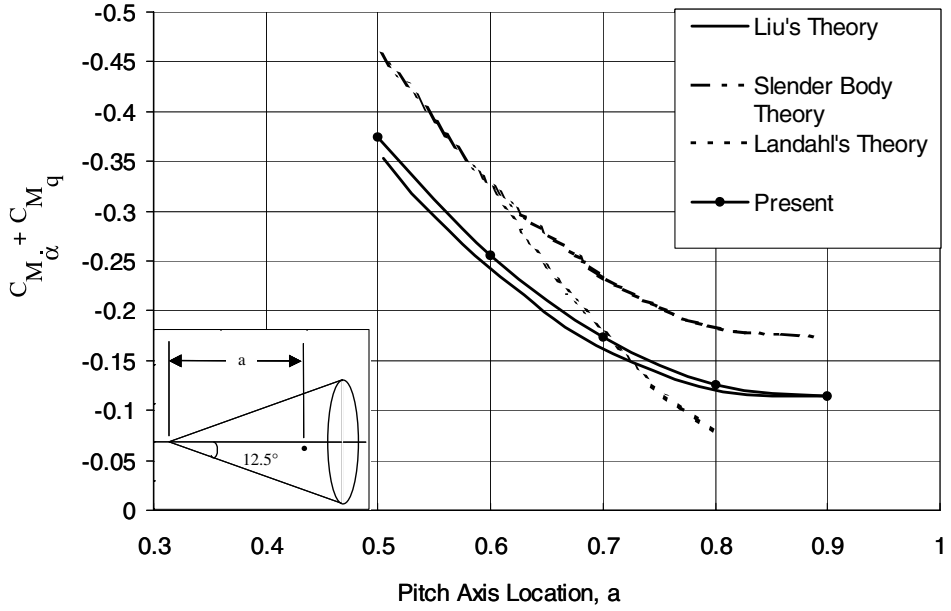

Fig. 7 Damping-in-pitch moment coefficient of a 12.5° cone with various pitch axes.

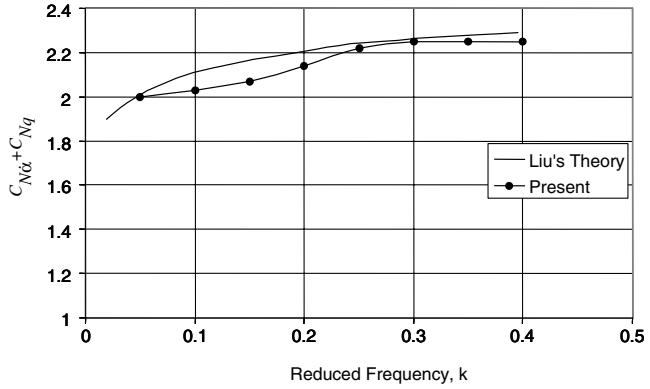

Fig. 8 Damping-in-pitch normal force coefficient for the cones of various cone angles at $M = 1.0$ with pitch axis location at the nose.

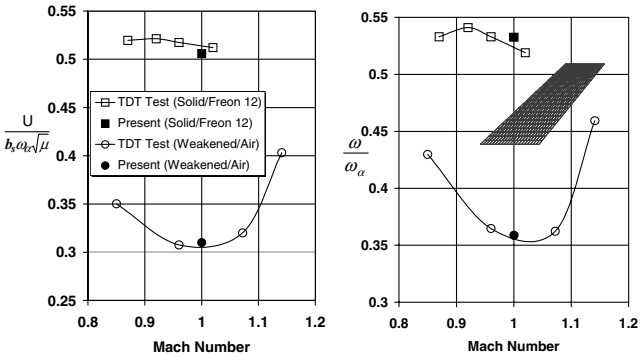

Fig. 9 Comparison of the ZSAP flutter solutions with test data of the AGARD 445.6 wing.

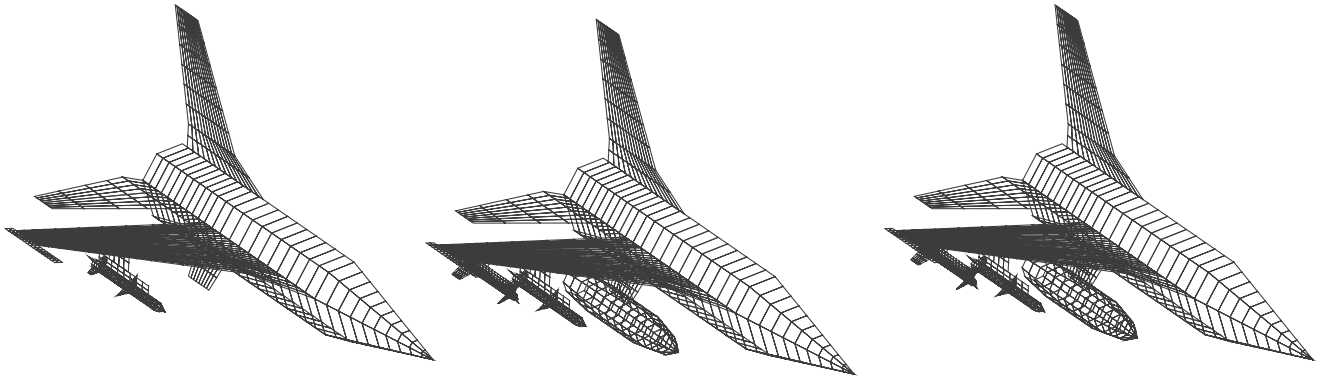

a) Classical flutter b) Typical LCO c) Non-Typical LCO

Fig. 10 ZSAP panel models of 3 F-16/store configurations.

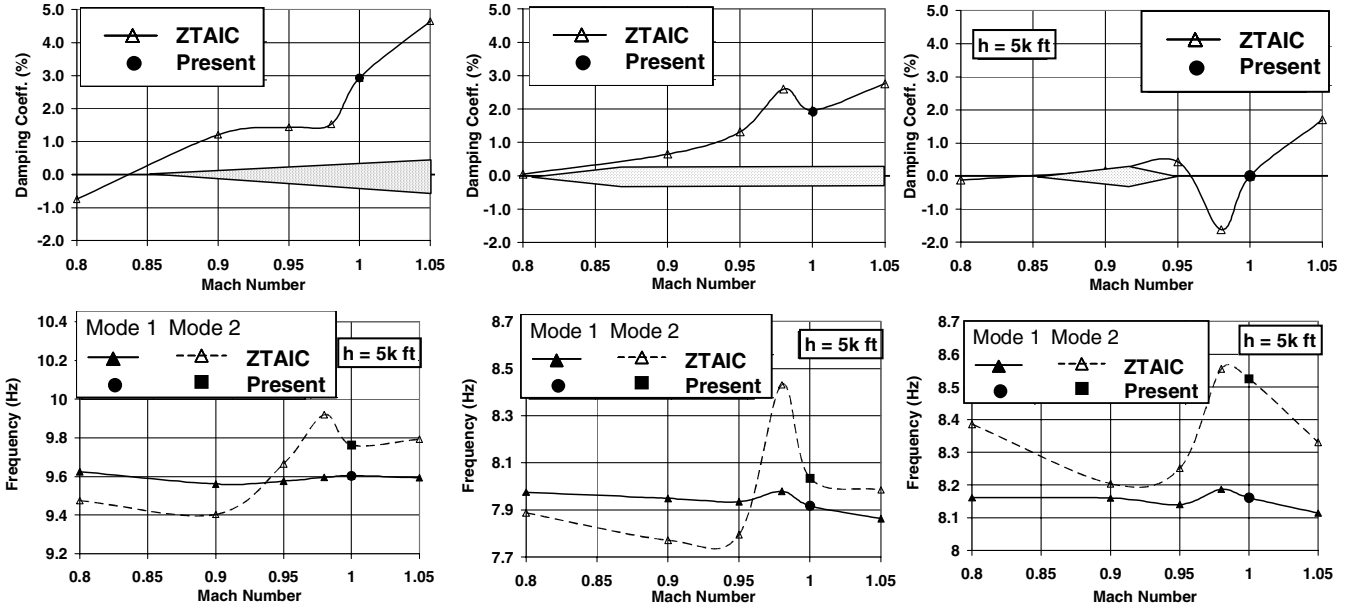

a) Classical Flutter b) Typical LCO c.) Non-typical LCO

Fig. 11 ZSAP flutter solution at Mach one and altitude = 5 kft of the 3 F-16/store configurations.

F-16 with External Stores

Three F-16 with external stores adopted from Denegri [30] are selected as the test cases for the ZSAP method. The ZSAP box models of these three cases are shown in Fig. 10 where the wing, pylons, and launches are modeled by the wing boxes, and the fuselage and store bodies are modeled by the body boxes. The detailed description of the store configurations and their associated F-16 weapon-carriage stations can be found in Denegri [30]. These three F-16/store configurations experienced different aeroelastic instabilities in flight tests; classified by Denegri [30] as classical flutter, typical limit cycle oscillation (LCO), and nontypical LCO whose flight regimes where the aeroelastic instabilities occur are shown by the double wedge symbol in Figs. 11a and 11b for classical flutter and typical LCO, respectively, and by the diamond symbol in Fig. 11c for nontypical LCO.

In Fig. 11, the flutter solutions computed by Chen et al. [25] using a transonic unsteady aerodynamic method called ZTAIC [1,31] are also presented. Based on a nonlinear damping criteria, Chen et al. has shown good correlations between the ZTAIC transonic flutter solutions and the flight test data. However, because ZTAIC solves the transonic small disturbance equation which breaks down at Mach one, the flutter solution at $M = 1$ is absent in Chen's results. Therefore, the objective of the present test cases is to provide the Mach-one flutter solutions using ZSAP and correlate the ZSAP solutions with the flight test data.

Also shown in Fig. 11 by the circle symbols is the ZSAP flutter solution for the three cases at $M = 1$. It can be seen that the ZSAP flutter damping and frequency solutions appear to fall onto the smooth lines connected by the ZTAIC solutions. In addition, the ZSAP flutter solution does correlate well with the flight test data of the three cases; unstable damping for the classical flutter and typical LCO cases indicating aeroelastic instability and stable damping for the nontypical LCO indicating the disappearance of LCO at Mach one. Again, this good correlation with flight test data is because of the low aspect and thickness ratio design of the F-16 wing where the semi-span-to-chord ratio $\hat{\sigma} \approx 0.84$ and thickness ratio $\tau \approx 0.04$ giving $\hat{\sigma}\tau\ \ell_n\ \hat{\sigma}^{-1}\tau^{-1/3} = 0.042$. Meanwhile the reduced frequencies of the ZSAP flutter solution are $k = 0.29$ for the classical flutter case, $k = 0.247$ for the typical LCO case and $k = 0.24$ for the nontypical LCO case which fully satisfy the inequality condition of Eq. (4).

Conclusions

Our renewed interest in the unsteady sonic-flow theory is motivated by the need of an expedient transonic method for ease of aeroelastic applications. The present sonic acceleration potential (ZSAP) method is a new development in the following aspects:

1) It is an acceleration potential approach whereby the computational domain only includes the wing planforms excluding the wake regions altogether.

2) Its source body panel formulation for arbitrary body modeling and the nonplanar wing panel formulation for lifting surface modeling allow the aeroelastic application for complex configurations such as whole aircraft with external stores.

3) Its panel discretization scheme is identical to that of ZONA6 and ZONA7, allowing all three methods to share the same panel model, thereby largely reducing the panel model generation effort.

Hence, the present method ZSAP should serve as the sonic counterpart of our unsteady transonic method ZTAIC for aeroelastic applications to lifting surfaces. It also bridges our wing-body methods through the subsonic-sonic-supersonic Mach number ranges. For modern supersonic/sonic aircraft, the low-drag requirement for high-speed cruise/maneuver usually results in a low-aspect ratio and thin airfoil, section design. For composite wing design it should further increase the wing stiffness. Given these design requirements, it is not surprising that our computed flutter solutions could be validated as they can largely satisfy Landahl's criterion. Thus it renders the present method ZSAP a very attractive tool for a wide-class of flutter and aeroelastic applications at sonic speed.

References

[1] Liu, D. D., Kao, Y. F., and Fung, K. Y., "An Efficient Method for Computing Unsteady Transonic Aerodynamics of Swept Wings with Control Surfaces," *Journal of Aircraft*, Vol. 25, No. 1, January 1988, pp. 25–31.

[2] Lu, S., and Voß, R., "TDLM: A Transonic Doublet Lattice Method for 3D Potential Unsteady Transonic Flow Calculations," DLR, German Aerospace Center DLR-FB 92-25, Göttingen, Germany, September 1992.

[3] Liu, D. D., and Winther, B. A., "Towards a Mixed Kernel Function Approach for Unsteady Transonic Flow Analysis," *AGARD Fluid Dynamics Panel Symposium on Unsteady Aerodynamics*, CP-227, AGARD, Neuilly Sur Seine, France, 1978, pp. 12-1–12-17.

[4] Oswatitsch, K., and Keune, F., "Flow Around Bodies of Revolution at Mach Number One," *Conference on High-Speed Aeronautics*, Polytechnic Institute of Brooklyn, Brooklyn, NY, 1955.

[5] Landahl, M. T., *Unsteady Transonic Flow*, Pergamon Press, Oxford, London, New York, Paris, 1961.

[6] Lin, C. C., Reissner, E., and Tsien, H. S., "On Two-Dimensional Non-Steady Motion of a Slender Body in a Compressible Fluid," *Journal of Mathematical and Physical Sciences*, Vol. XXVII, No. 3, 1948, pp. 220–231.

[7] Rott, N., "Oscillating Airfoils at Mach Number One," *Journal of Aeronautical Sciences*, Vol. 16, No. 6, 1949, pp. 380–381.

[8] Liu, D. D., Platzer, M. F., and Ruo, S. Y., "Unsteady Linearized Transonic Flow Analysis for Slender Bodies," *AIAA Journal*, Vol. 15, No. 7, July 1977, pp. 966–973.

[9] Kimble, K. R., Liu, D. D., Ruo, S. Y., and Wu, J. M., "Unsteady Transonic Flow Analysis for Low Aspect Ratio, Pointed Wings," *AIAA Journal*, Vol. 12, No. 4, 1974, pp. 516–522.

[10] Runyan, H. L., and Woolston, D. S., "Method for Calculating the Aerodynamic Loading on Oscillating Finite Wing in Subsonic and Sonic Flow," NACA, Rept. 1322, 1957.

[11] Davies, D. E., "Three-Dimensional Sonic Theory," *AGARD Manual on Aeroelastcity, Part 2: Aerodynamic Aspects*, AGARD, Neuilly Sur Seine, France, 1959, Chap. 4; also Rept. AD274-097

[12] Rodemich, E. R., and Andrew, L. V., "Unsteady Aerodynamics for Advanced Configurations: A Transonic Box Method for Planar Lifting Surfaces," Pt. 2, Air Force Flight Dynamics Laboratory TDR-64-152, May 1965.

[13] Olsen, J. J., "Demonstration of a Transonic Box Method for Unsteady Aerodynamics of Planar Wings," Air Force Flight Dynamics Laboratory TR-66-121, Oct. 1966.

[14] Ruo, S. Y., and Theisen, J. G., "Calculation of Unsteady Transonic Aerodynamics for Oscillating Wings with Thickness," NASA CR 2259, June 1975.

[15] Soviero, P. A. O., and Cesar, G. A. V., "Swept Thin Wings in Unsteady Sonic Flow," *AIAA Journal*, Vol. 39, No. 9, September 2001, pp. 1798–1799.

[16] Stahara, S. S., and Sprieter, J. R., "Research on Unsteady Transonic Flow Theory," Nielsen Engineering and Research TR 107, January 1976.

[17] Chen, P. C., Lee, H. W., and Liu, D. D., "Unsteady Subsonic Aerodynamics for Bodies and Wings with External Stores Including Wake Effort," *Journal of Aircraft*, Vol. 30, No. 5, Sept.–Oct. 1993, pp. 618–628.

[18] Chen, P. C., and Liu, D. D., "Unsteady Supersonic Computation of Arbitrary Wing-Body Configurations Including External Stores," *Journal of Aircraft*, Vol. 27, No. 2, Feb. 1990, pp. 108–116.

[19] Garcia-Fogeda, P., Chen, P. C., and Liu, D. D., "Unsteady Supersonic Flow Calculations for Wing-Body Combinations Using Harmonic Gradient Method," *AIAA Journal*, Vol. 28, No. 4, 1990, pp. 635–641.

[20] Laschka, B., "Zur Theorie der Harmonisch Schwingenden Tragenden Fläche bei Unterschallanstromung," *Zeitschrift fur Flugwissenschaften*, Vol. 11, No. 7, 1963, pp. 265–292.

[21] Desmarais, R. M., "An Accurate and Efficient Method for Evaluating the Kernel of the Integral Equation Relating Pressure to Normal Wash in Unsteady Potential Flow," AIAA Paper 82-0687, April 1982.

[22] Soveriero, P. A. O., and Pinto, F. H. L. "Unsteady Lifting Surface Theory in Sonic Flow: The Problem Revisited," *AIAA Journal*, Vol. 38, No. 5, May 2000, pp. 931–933.

[23] Abramowitz, M., and Stegan, I. A. "*Handbook of Mathematical Functions*," Dover Publications Inc., New York, 1965, p. 299.

[24] Rodden, W. P., Giesing, J. P., and Kalman, T. P., "New Method for Nonplanar Configurations," *AGARD Conference Proceedings*, CP-80-71, Pt. 2, No. 4, AGARD, Neuilly Sur Seine, France, 1971.

[25] Chen, P. C., Sulaeman, E., Liu, D. D., and Denegri, C. M., Jr., "Influence of External Store Aerodynamics on Flutter/LCO of a Fighter Aircraft," *43rd AIAA/ASME/ASCE/AHS/ASC Structural Dynamics and Materials Conference*, AIAA Paper 2002-1410, April 2002.

[26] Stark, V. J. E., "Canard-Wing Interaction in Unsteady Supersonic Flow," *Journal of Aircraft*, Vol. 26, No. 10, 1989, pp. 951–952.

[27] Liu, D. D., "Quasi-Slender Body Theory for Unsteady Linearized Transonic Flow Past Pointed Bodies of Revolution," Lockheed Missiles and Space Company LMSC/HREC A791435, Huntsville, AL, April 1968.

[28] Landahl, M. T., "Forces and Moments on Oscillating Slender Wing-Body Combinations at Sonic Speed," U.S. Air Force Office of Scientific Research Rept. OSR-TN-56-109, 1956.

[29] Yates, E. C., "AGARD Standard Aeroelastic Configurations for Dynamic Response I-Wing 445.6," AGARD, Rept. 765.

[30] Denegri, C. M., Jr., "Limit Cycle Oscillation Flight Test Results of a Fighter with External Stores," *Journal of Aircraft*, Vol. 37, No. 5, Sept.–Oct. 2000, pp. 761–769.

[31] Chen, P. C., Sarhaddi, D., and Liu, D. D., "Transonic Aerodynamic-Influence-Coefficient Approach for Aeroelastic and MDO Applications," *Proceedings of the Euromech Colloquium 349 at DLR*; also in *Journal of Aircraft*, Vol. 37, No. 1, Jan.–Feb. 2000, pp. 85–94.

E. Livne
Associate Editor